

Ionization of N₂ in collisions with fast electrons: Evidence of an interference effectMadhusree Roy Chowdhury,¹ C. R. Stia,² C. A. Tachino,² O. A. Fojon,² Roberto D. Rivarola,² and Lokesh C. Tribedi^{1,*}¹Tata Institute of Fundamental Research, Colaba, Mumbai 400005, India²Institute de Fisica Rosario (CONICET-UNR), Universidad Nacional de Rosario, 2000 Rosario, Argentina

(Received 21 August 2016; published 14 November 2016)

Absolute double differential cross sections (DDCS) of electron emission were measured for ionization of N₂ by fast electrons with energy 7 keV. Measurements were performed for different electron emission angles and energies. Evidence of oscillation due to Young-type interference was observed in the DDCS ratios for all angles. The frequency for large backward angle is found to be larger compared to that for small forward angle. Consequently, the forward-backward asymmetry parameter reveals the oscillatory structure even more clearly. The oscillations observed for both experimental-to-theoretical DDCS ratios and forward-backward asymmetry were well explained by the Cohen-Fano model of interference in a molecular double slit. A periodic deviation of the Cohen-Fano model from the asymmetry parameter data reveals the presence of a higher-frequency component. The first Born model was employed to explain the results of molecular nitrogen for which a complete-neglect-of-differential-overlap approximation was used along with an effective atomic number.

DOI: [10.1103/PhysRevA.94.052703](https://doi.org/10.1103/PhysRevA.94.052703)**I. INTRODUCTION**

Electron-impact ionization of atoms and molecules is an important field in the study of basic atomic collision physics. There have been numerous experimental and theoretical investigations in this field for many decades. Many aspects of electron-induced ionization are being investigated, such as total cross sections, single and double differential cross section (DDCS), e-2e and e-3e collision processes, as well as double and multiple ionizations [1,2]. The e-DDCS spectrum carries rich information regarding the collision mechanisms compared to the single differential and total cross sections. Such measurements of the absolute cross sections at the DDCS level are scarce, although it has major applications in other fields, such as plasma physics, astrophysics, cluster physics, and, in general, atomic collision physics involving photons, electrons, and ions as projectiles.

However, other fundamental processes which have implications for basic quantum physics, such as Young-type electron interference from a molecular double slit which is a relatively new feature, can be well investigated from an electron DDCS spectrum arising from such collisions. Such an interference and the resulting oscillation in the electron spectrum was predicted by Cohen and Fano in 1966 [3]. Investigation of the interference effect in the electron emission spectrum arising from a diatomic molecule in collision with photons, electrons, and fast heavy ions has been the subject of intensive experimental and theoretical studies. For homonuclear diatomic molecules, since the two atomic centers are indistinguishable, the probability of electron emission from either atom is expected to add coherently, resulting in an interference effect. The two atoms are analogous to the two slits in Young's double-slit experiment on light scattering, which played a major role in the formation and progress of quantum mechanics.

Experiments on ionization of H₂ by heavy ions, electrons, and photons [4–11] were performed to investigate the interference effect. Similarly, other diatomic molecules, such as

N₂, O₂, and CO [11–23], have been the subject of study in recent years to look for an interference effect. Although in the case of H₂, evidence of an interference effect was seen for both heavy-ion and electron impact, for multielectronic targets such as O₂ and N₂, there is an ambiguity in such observation in the case of heavy-ion impact. For the N₂ molecule, the oscillation which was observed by proton impact [12] has been interpreted to have the signature of a second-order scattering process only. On the other hand, in the case of H₂, a double-collision model was used [24,25] to explain the observed double-frequency component (second-order process), along with the presence of a first-order Cohen-Fano oscillation. According to the continuum distorted wave-eikonal initial state (CDW-EIS) model [26], for proton impact ionization of N₂, oscillations are visible in individual orbitals, which are phase shifted from each other. Thus, adding up the contributions from all orbitals leads to the cancellation of intensities and therefore the DDCS spectra may not reveal any signature of oscillation. The recent experimental work on the DDCS measurement of N₂ [16] did not show any appreciable oscillation, also for O₂, where no oscillation was observed [17]. On the contrary, Ilchen *et al.* [18] demonstrated the existence of interference oscillation in photoionization of 1σ_g and 1σ_u orbitals of N₂ molecule. There exists a phase mismatch in the oscillations of these two individual orbitals. Similarly, interference oscillation was observed clearly in the vibrationally resolved states of N₂ [11].

Fast electrons impart much weaker perturbation to the target as compared to fast heavy ions during collision. It is well known that heavy ions cause simultaneous multiple ionization of outer shells of atoms along with single ionization. Thus, multiple ionization of different orbitals complicates the process, which as a result may create difficulty in observing the oscillations. In the case of fast electron collisions, the probability of multiple ionization is much less compared to that for heavy-ion collisions [27]. In this work, we present the DDCS spectra of the secondary electrons ejected due to the collision of fast electrons with N₂ and a clear signature of first-order interference effect is visible from the DDCS ratios, which is in partial agreement with the observation in [14]. The DDCSs are measured as a function of emitted electron

*lokesh@tifr.res.in; ltribedi@gmail.com

energy and angle. The forward-backward angular asymmetry parameter and the details of the interference oscillation are deduced from the measured DDCS spectra.

II. EXPERIMENTAL DETAILS

We present a brief sketch of the experimental setup used for the measurement of energy and angular distributions of the secondary electrons. The experiment has been performed with a 7 keV (projectile velocity $v_p \sim 22.7$ a.u.) electron beam obtained from a commercially available electron gun. These fast electrons were initially focused using a set of einzel lens and deflectors present within the electron gun assembly. Electron being a light mass particle and the distance between the electron gun filament and interaction region in the scattering chamber being quite large (~ 1.5 m), one set of lens and deflectors was not sufficient to get a well-collimated parallel beam near the interaction region. Another set of einzel lens, a pair of electrostatic deflectors, and a collimator stack with three collimators were incorporated in the beam line to focus the beam. The last aperture of 2.5 mm diameter was used to cut the beam before it reached the interaction region. For better alignment, two sets of magnetic coils were also introduced in the beam line. Finally, a well-collimated parallel beam was directed to the N_2 target gas present in the scattering chamber. The beam current was typically around 900 nA, which remained almost stable throughout the experimental process with minor fluctuation in the presence and absence of gas.

The collision processes took place in a high vacuum scattering chamber made of stainless steel having diameter of 18 inches. It is equipped with a motorized turntable and a hemispherical electrostatic analyzer. A base pressure of 7×10^{-8} mbar was achieved with a 2000 l/sec turbo molecular pump backed by a triscroll pump. The chamber was flooded with the target gas (molecular nitrogen) at an absolute pressure of 0.15 mTorr, which was measured by a capacitance manometer (MKS Baratron). The Earth's magnetic field was reduced to about 5–10 mGauss near the interaction region by placing two μ metal sheets on the inner side of the scattering chamber. In addition, it was also ensured that the electric and magnetic field due to the lens and deflectors in the beam line did not have any effect on the emitted secondary electron spectrum, particularly for the low-energy electrons. The electrons ejected from the target after the collision process were energy analyzed by the hemispherical electrostatic analyzer sitting on the turntable. The hemispherical analyzer has an inner and outer diameter of 25 and 35 mm, respectively. A preacceleration voltage of 6 V was applied at the entrance and exit slit of the spectrometer to enhance the collection efficiency of the low-energy electrons (< 5 eV) which otherwise may be deflected by the presence of any stray electric or magnetic field near the interaction region. The energy-analyzed electrons were detected by a channel electron multiplier (CEM) placed after the exit slit of the hemispherical analyzer. The cone of the CEM was kept at a positive potential of 100 V because the detection efficiency of the CEM remains constant (0.85) for electron energies between 100–500 eV, as obtained from the operation manual of the detector. Since the chamber is flooded with target gas, the collision volume is extended along the electron beam and therefore the acceptance angle of the

analyzer varies between 3.4° to 3.6° based on the emission angle. The corresponding estimated average uncertainty in electron emission angle is about 3.7° . Energy resolution of the analyzer is about 6% in which the contribution due to the acceptance angle is about 1% (see Ref. [28]). At each energy, the number of electrons ejected were detected for a specified amount of incident projectile charge collected on a Faraday cup. A LABVIEW-based data acquisition system was used for scanning the voltages on the hemispheres and to collect the data for different electron energies.

The secondary electrons having energies of 1–550 eV were detected for different angles from 15° to 145° . The error due to statistical fluctuation was low (4%–6%) throughout the experiment. Gas pressure fluctuation was about 6% to 7%. The maximum absolute error in the data for the present experiment was about 15%.

III. THEORETICAL MODELS

The DDCS of ionization of N_2 molecules is obtained by the method proposed by Senger *et al.* [29], developed in the framework of the complete neglect of differential overlap (CNDO) approximation [30]. Briefly, molecular orbitals (MOs) are constructed from a linear combination of atomic orbitals in a self-consistent field approach by using a minimal basis size: only atomic orbitals of those which are occupied in the ground state of the atoms of the molecule are utilized. In this treatment, the weight of such atomic contributions is expressed in terms of the electronic population.

For the ground state of the N_2 molecule, the electronic configuration is $(N 1s)^4 (\sigma_g 2s)^2 (\sigma_u 2s)^2 (\pi_u 2p)^4 (\sigma_g 2p)^2$. The contribution of the different atomic states to the MO extracted from Ref. [31] is shown in Table I, as well as the corresponding measured MO binding energies taken from Ref. [32]. As a consequence, in the monocentric CNDO model, the DDCS for a particular MO reduces to a sum of the cross sections for N atomic compounds weighted by the weights resulting from the Mulliken population analysis for the considered MO (see Table I) [29]. The total DDCS for the molecule is obtained then as a sum of all MO contributions.

The electronic configuration of the ground state $^4S_{3/2}$ of the N atom is $(1s)^2(2s)^2(2p)^3$. Within the framework of an independent electron model, the multielectronic problem is reduced to a single-electron one under the following assumption. It is supposed that one of the target electrons (the *active* electron) is ionized in the final channel of the reaction, whereas the other ones (the *passive* electrons) remain as frozen in their initial orbitals. Hence, no appreciable relaxation of the target is assumed during the effective collision time, which is

TABLE I. Population and experimental binding energies of the N_2 molecular orbitals (MOs).

MO	Population [31]	Expt. energy (eV) [32]
N 1s	4.00 N 1s	−409.90
$\sigma_g 2s$	1.50 N 2s + 0.50 N 2p	−37.23
$\sigma_u 2s$	1.47 N 2s + 0.53 N 2p	−18.60
$\pi_u 2p$	4.00 N 2p	−16.80
$\sigma_g 2p$	0.5 N 2s + 1.50 N 2p	−15.50

justified as the latter is much less than the relaxation time of the target at the impact energies of interest [33].

The DDCCS for a particular orbital of the N target is obtained from the following expression:

$$\frac{d^2\sigma}{d\Omega_e dE_e} = (2\pi)^4 \frac{k k_s}{k_i} \int d\Omega_s |t_{fi}|^2, \quad (1)$$

where \mathbf{k} and \mathbf{k}_s are the momenta of the *active* ejected electron and the scattered one, respectively, whereas $d\Omega_e$ and $d\Omega_s$ represent the corresponding differential solid angles with respect to the incidence direction defined by the incident-electron momentum \mathbf{k}_i . Moreover, $E_e = k^2/2$ is the energy of the emitted electron.

The *prior* version of the transition-matrix element reads

$$t_{fi} = \langle \psi_f^- | V_i | \psi_i \rangle, \quad (2)$$

where ψ_i is the wave function in the initial channel and ψ_f^- is the final wave function with correct asymptotic conditions. V_i is the perturbation in the entrance channel.

The initial wave function is chosen as a product between a plane wave for the incident projectile and a bound-state wave function ϕ_j for the active electron,

$$\psi_i = \frac{e^{i\mathbf{k}_i \cdot \mathbf{R}}}{(2\pi)^{3/2}} \phi_j(\mathbf{r}), \quad (3)$$

where \mathbf{R} and \mathbf{r} are the position vectors of the incident electron and the active electron, respectively. Atomic orbitals ϕ_j ($j = 1s, 2s, 2p$) are described here within the Roothaan-Hartree-Fock approximation [34].

In the first Born approximation, the final-state wave function is chosen as

$$\psi_f^- \cong \frac{e^{i\mathbf{k}_f \cdot \mathbf{R}}}{(2\pi)^{3/2}} C(\mathbf{k}, \mathbf{r}, \gamma), \quad (4)$$

where

$$C(\mathbf{k}, \mathbf{r}, \nu) = \Gamma(1 - i\gamma) \frac{e^{i\mathbf{k} \cdot \mathbf{r}}}{(2\pi)^{3/2}} e^{-\pi\gamma/2} \times {}_1F_1[i\gamma; 1; -i(kr + \mathbf{k} \cdot \mathbf{r})] \quad (5)$$

describes the ionized electron in the field of the residual target at asymptotically large distances. ${}_1F_1$ is the confluent hypergeometric function and $\gamma = -Z_T/k$ is the corresponding Sommerfeld parameter. Here, Z_T is an effective charge corresponding to the residual target *seen* by the active electron.

According to the choice of the initial state, the perturbation V_i in the initial channel is taken as

$$V_i = \frac{1}{r_p} - \frac{1}{R}, \quad (6)$$

where $\mathbf{r}_p = \mathbf{r} - \mathbf{R}$ is the position vector of the active electron with respect to the projectile. The perturbation V_i corresponds to the interaction of the projectile with the *active* electron and with a net charge equal to unity. This is compatible with the complete screened charge of the nuclei by the *passive* electrons.

In order to evaluate the influence of the passive electrons in the final channel, either an asymptotic charge $Z_T = 1$, which corresponds to a total screening of the nucleus, or

$Z_T = Z_{bk} = \sqrt{-2n_j^2\epsilon_j}$ [35] is used in the DDCCS calculations for both N and N₂ targets. For the case of atomic cross-section calculations, ϵ_j is the Roothaan-Hartree-Fock energy [34], whereas for N₂ computations, ϵ_j represents the MO energies shown in Table I. In both cases, n_j is the principal quantum number of the atomic orbital involved in the calculations. Further details can be found in Ref. [36].

IV. RESULTS AND DISCUSSIONS

In this section, the experimentally observed DDCCS spectra for the N₂ target and consequently the interference oscillations obtained from the DDCCS ratios are discussed along with the forward-backward asymmetry.

A. Energy distribution of electron DDCCS at fixed emission angles

The measured absolute electron DDCCSs for N₂ as a function of emitted electron energy for four different emission angles are shown in Fig. 1. The theoretical cross sections for N₂ and 2N, calculated using effective charges $Z_T = 1$ and $Z_T = Z_{bk}$, are also plotted. From the figure, it is seen that the cross section decreases over four orders of magnitude in the measured electron energy range. In the low-energy part of the spectrum, the cross section reaches a maximum due to the contribution from the soft electron emission process where the momentum transfer is small and the electrons are emitted with very large impact parameter. The calculations for N₂ and 2N are seen to merge almost completely for either values of Z_T . The calculation with $Z_T = 1$ matches with the experimental data qualitatively, but overestimates it for all angles. The calculation corresponding to Z_{bk} is seen to have better agreement with data beyond 20 eV for all angles. For extreme backward angles, $Z_T = Z_{bk}$ underestimates the data. In the low-energy region,

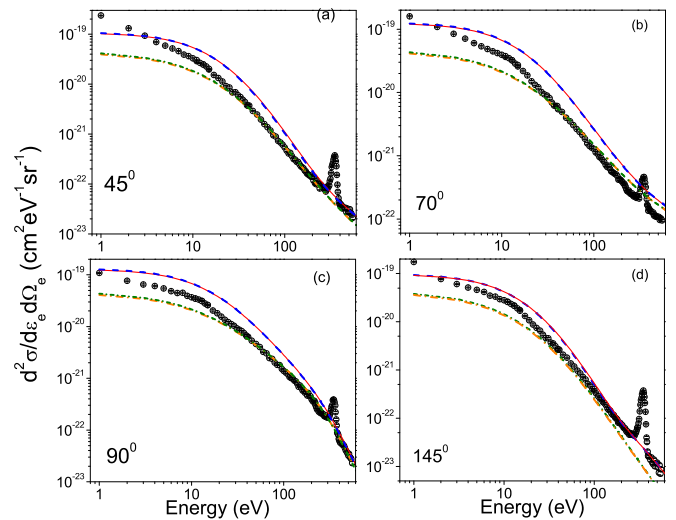


FIG. 1. Absolute DDCCS for different emission angles: Theoretical cross sections for N₂ (red solid line) and 2N (blue dashed line) corresponding to $Z_T = 1$ are displayed. The calculations using $Z_T = Z_{bk}$ are also shown by the orange dash-dotted line (N₂) and green dotted line (2N). The calculations for N₂ and 2N, being almost identical, cannot be distinguished.

the discrepancy between data and theoretical calculation using Z_{bk} is larger in the case of forward angles compared to the backward angles. The sharp peak observed at about 355 eV corresponds to the K-LL Auger electron emission, which is not taken into account in the theoretical calculations. The DDCS for N_2 (under dipole approximation) can be written as [4]

$$\sigma_{N_2}(k, \theta) = \sigma_{2N}(k) \left[1 + \frac{\sin[kc(\theta)d]}{kc(\theta)d} \right]. \quad (7)$$

Here, k represents the electron momentum in a.u. and d is the internuclear distance (2.1 a.u. for N_2). The quantity $c(\theta)$ is an adjustable frequency parameter, and the term $\frac{\sin[kc(\theta)d]}{kc(\theta)d}$ is known as the Cohen-Fano term [3,4,37]. The DDCS for 2N (σ_{2N}) was obtained from theoretical calculations. The ratio $\text{DDCS}(N_2)/2\text{DDCS}(N)$ shows the interference oscillation, which is discussed in the following section.

B. Angular distribution of electron DDCS at fixed emission energies

Figure 2 displays the angular distribution of DDCS for different electron emission energies. An absolute error of 15% is shown for some data points. The four theoretical curves correspond to the cross sections for N_2 and 2N with the effective charge $Z_T = 1$ and $Z_T = Z_{bk}$. The theoretical calculations match qualitatively with the data, but $Z_T = 1$ overestimates the measured values in all cases. The calculations with Z_{bk} underestimate the data for 9 eV, but match qualitatively for higher energies. A closer inspection into the plots for 120 and 200 eV show that the curves for $Z_T = Z_{bk}$ are below the measured values for extreme forward and backward angles. In the case of low emission energies, the distributions are almost flat, but with the increase in electron emission energy, the distributions gradually show a peaking structure around 80° . This difference in the shape of the distribution for low and high energy is understood in terms of the binary nature of collisions. Further, from the figure it is readily seen that for lower electron energies, the DDCS values are almost the same for extreme forward and backward angles. However, with the increase in energy, the DDCS for forward angles is

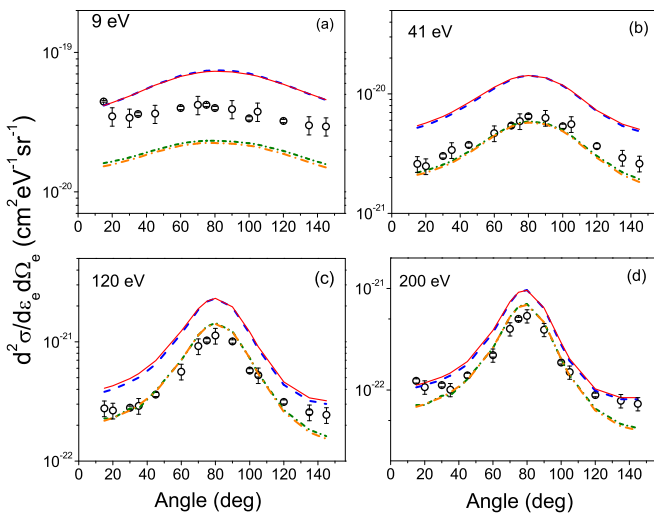


FIG. 2. Absolute DDCS for fixed electron emission energies. Legends are similar to that mentioned in Fig. 1.

slightly greater than for backward angles. This behavior is also reproduced qualitatively by the theoretical calculations, although they do not match quantitatively with data. It can be inferred that there is only minor signature of forward-backward angular asymmetry in the case of electron-impact collisions.

C. DDCS ratios

1. Experimental-to-theoretical DDCS ratios

As seen from Fig. 1, the DDCSs for N_2 and independent N atoms fall by several orders of magnitude with the electron energy, whereas the variation due to the interference effect is rather small. To enhance the visibility of interference oscillation, it is essential to omit the variation of cross section with electron energy. Therefore, the DDCS for N_2 should be divided by the corresponding DDCS of the two N atoms. In the absence of experimental data for atomic N, the experimental DDCSs for N_2 were divided by theoretical DDCS for 2N, which has been calculated using the effective charges $Z_T = 1$ and $Z_T = Z_{bk}$. Figures 3 and 4 show the DDCS ratios obtained using $Z_T = 1$ and $Z_T = Z_{bk}$, respectively. In Fig. 3, a half sinusoidal oscillatory structure is observed about a horizontal line around a value of 0.5 forward angles and around 0.6 for 145° . The oscillations are expected to be around a horizontal line near 1.0, but as seen from Fig. 1, the calculations using $Z_T = 1$ overestimate the measured data for all angles, resulting in the oscillations being observed below 1.0. In the case of 145° , the oscillation frequency is seen to be much higher compared to the other angles. The ratios are fitted by the Cohen-Fano-type function (shown by solid lines in Fig. 3) given by

$$\sigma_{\text{norm}}(k, \theta) = A + F \frac{\sin[kc(\theta)d]}{kc(\theta)d}, \quad (8)$$

where $\sigma_{\text{norm}}(k, \theta)$ represents the DDCS ratio, i.e., $(\sigma_{N_2}/\sigma_{2N})$. The fitted curve matches quite well with the ratios except for 145° , where large discrepancy can be observed beyond 2.5 a.u. Such mismatch may be ascribed to the difference between the measured data and theory for 2N.

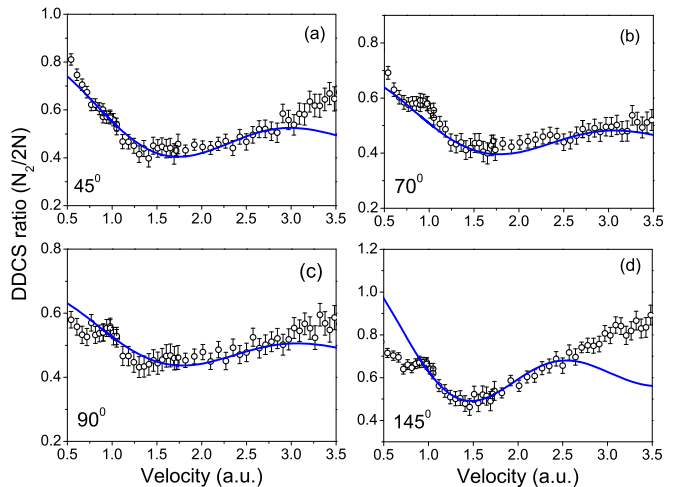


FIG. 3. Experimental-to-theoretical DDCS ratios (σ_{N_2}/σ_{2N}) at different scattering angles for $Z_T = 1$. The solid line corresponds to the analytical fitting function given in Eq. (8).

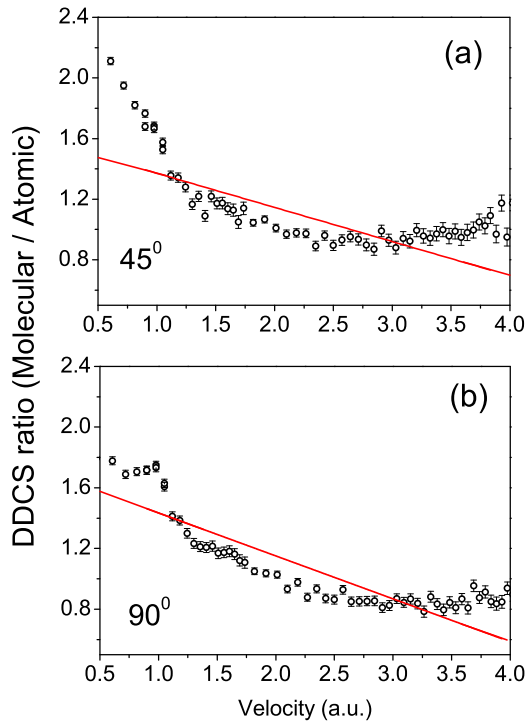


FIG. 4. Ratio of N₂ DDCS to twice atomic nitrogen DDCS obtained using $Z_T = Z_{bk}$ for atomic N cross section. The solid line corresponds to a linear function of negative slope used for fitting the ratios.

Figure 4 shows similar DDCS ratios which have been obtained using the effective charge $Z_T = Z_{bk}$ for 2N. The ratios show an oscillatory structure overriding on a straight line of negative slope. To reveal the oscillations clearly, a linear function (shown by the red line) was fitted to the ratios. The cross-section ratios were then divided by the fitted line and the resulting DDCS ratios are shown by the blue circles in Fig. 5 for four different angles. The linear fitting was performed to observe the oscillation about a horizontal line. Half sinusoidal oscillatory structures are observed around a horizontal line

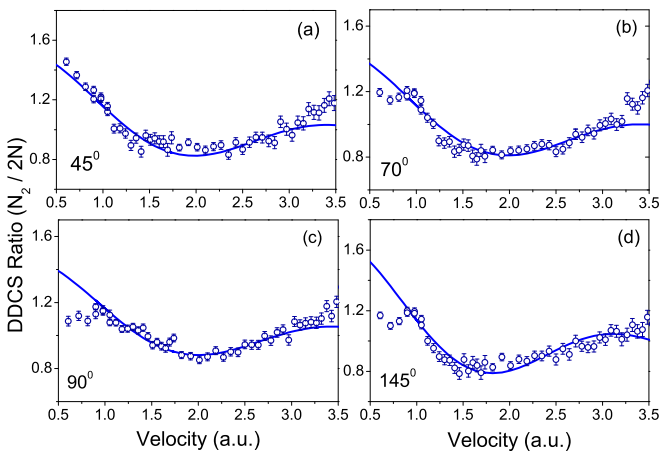


FIG. 5. DDCS ratios (σ_{N_2}/σ_{2N}) obtained after dividing by the linear fitted line in Fig. 4. The solid curve shows the fitting function given in Eq. (8).

near 1.0 for all the angles. This oscillatory behavior, thus, is qualitatively similar to that observed using $Z_T = 1$, as shown in Fig. 3. The ratios were further fitted by the Cohen-Fano function given in Eq. (8). It is seen that the fitted function (shown by the blue solid line) has a good agreement with the experimental-to-theoretical ratios.

The choice of effective charge Z_T for calculating the atomic N cross sections plays a crucial role in determining the shape of the oscillations in the DDCS ratios, as seen in Figs. 3 and 4. Though, from Fig. 1, a better agreement is observed between the measured DDCS of N₂ with that of 2N using $Z_T = Z_{bk}$ at higher energies, the ratios do not reveal proper oscillation. The oscillation, about a horizontal line, is finally revealed only after dividing by a fitted straight line. On the other hand, for the DDCS for 2N using $Z_T = 1$, although it overestimates the N₂ cross section (Fig. 1), it provides clearer oscillation about a horizontal line.

It should be mentioned here that the relative N₂/N triple-differential cross section (TDCS) of Ref. [14] shows clear structure, although the agreement with the Cohen-Fano factor is a bit poor at such lower-impact energy (250 eV), compared to the high-energy electron beam used in this experiment. Also we should note that in Ref. [14], the experiments and calculations are done only for the $3\sigma_g$ orbital, whereas our experimental results are presented for all molecular orbitals. We know from the case of ion impact that the interference effect can be shadowed [16,17,26] when the sum of all orbital contributions is included. The remarkable result obtained in our work is that the signature of interference patterns appears for the DDCS ratio considering the contributions of all molecular orbitals. This is possibly due to the fact that simultaneous multiple ionization of different orbitals is much less in the case of fast electron-impact ionization, compared to that for heavy-ion collisions in Refs. [16,17].

2. Frequency parameter

The variation of the angle-dependent frequency parameter $c(\theta)$ [obtained from the fitting function in Eq. (8)] as a function of electron emission angles is displayed in Fig. 6. It is seen that for all of the forward angles, frequency remains

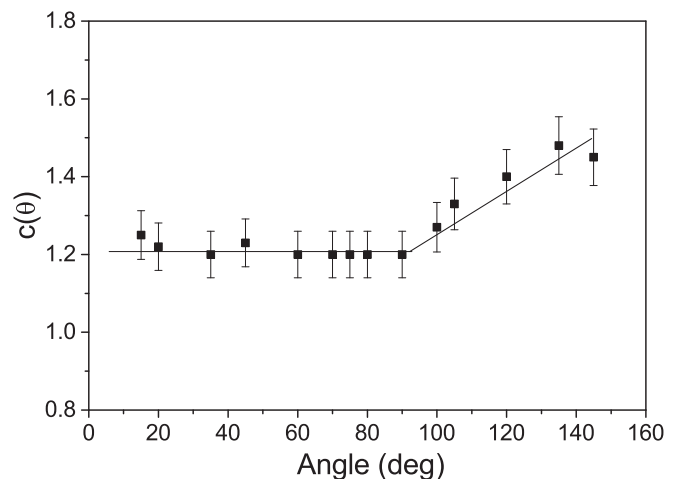


FIG. 6. Frequency parameter $c(\theta)$ plotted as a function of electron emission angle. The solid line is to guide the eyes.

almost constant up to 90° . In the case of backward angles, the frequency parameter increases steadily with the increase in the observation angle. The frequency parameter changes from a value of 1.2 to 1.45 over the entire angular range, giving an enhancement of a factor of about 1.20(8). The shape of the angular dependence of $c(\theta)$ is quite different than that for H_2 [8]. N_2 is a multielectronic target, and therefore ionization is possible from different molecular orbitals and hence some difference can be expected in the observed oscillation parameters compared to that for the simplest molecule, i.e., H_2 .

3. Forward-backward angular asymmetry

In the previous section, we have obtained the interference oscillation from the ratio of the experimental DDCS for N_2 to that of theoretical DDCS for atomic nitrogen. From Figs. 3 and 4, it is inferred that the pattern of interference oscillation depends on the choice of effective charge Z_T used for atomic N calculations. Another possible way to deduce the oscillation is from the asymmetry parameter according to the prescription given in [38]. In this method, the oscillation is directly determined from the ratios of the measured DDCS and hence does not depend on the absolute normalization procedure. In addition, since it involves the DDCS for the molecular target only, it is also free from atomic cross section and the choice of any effective charge. According to [39], non-Coulombic potential for a multielectronic atom or molecule contributes to the forward-backward asymmetry. In the case of a diatomic molecule, the Young-type interference can also influence the asymmetry parameter, as shown in Refs [7,38,40]. The asymmetry parameter $\alpha(k)$ is defined as

$$\alpha(k) = \frac{\sigma(k, \theta) - \sigma(k, \pi - \theta)}{\sigma(k, \theta) + \sigma(k, \pi - \theta)}, \quad (9)$$

where k is momentum and θ is chosen to be a small forward angle, 35° . As shown by Fainstein *et al.* [39], expanding $\sigma(k, \theta)$ in terms of the Legendre polynomials and considering the first few terms of the series expansion, $\alpha(k)$ represents the asymmetry parameter for $\theta = 0$. Since the variation of angular distribution around 0 and π is very small, we have used $\theta = 35^\circ$ in the present case to calculate $\alpha(k)$ approximately. The asymmetry parameter, obtained from the molecular DDCS for two complementary angles, is shown in Fig. 7 as a function of electron velocity. The quantity $\alpha(k)$ shows a full sinusoidal oscillation with a minor increasing trend in the ejected electron velocity range of 0.6 to 3.5 a.u. From Fig. 6, we have seen that the frequency of oscillations is greater for backward angles compared to forward angles. This difference in frequency for two complementary angles give rise to the oscillatory structure in $\alpha(k)$. By replacing the DDCS in Eq. (9) with that in Eq. (7), which contains the Cohen-Fano term, one gets an expression for the asymmetry parameter $\alpha(k)$ as follows [40]:

$$\alpha(k) = \frac{k\beta c(\theta)d(A-B) + \{A\beta \sin[kc(\theta)d] - B \sin[k\beta c(\theta)d]\}}{k\beta c(\theta)d(A+B) + \{A\beta \sin[kc(\theta)d] + B \sin[k\beta c(\theta)d]\}}, \quad (10)$$

where electron energy $\epsilon_k = k^2/2$, A and B are the amplitudes of oscillation for the two complementary angles, d is the internuclear distance, $c(\theta)$ is the frequency of low forward

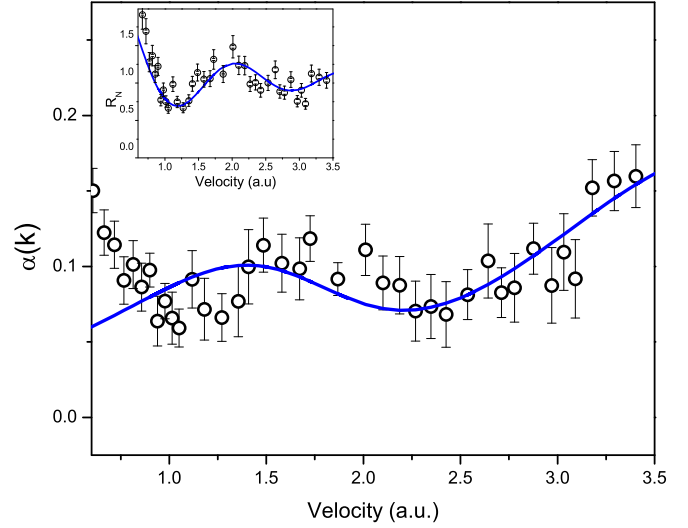


FIG. 7. Forward-backward asymmetry parameter obtained from measured DDCS of N_2 for low forward angle (35°) and large backward angle (145°). The solid line corresponds to the model fitting given by Eq. (10). Inset: asymmetry parameter divided by first-order fitting function.

angle having θ ($= 35^\circ$ in this case), and β is the ratio of oscillation frequency for backward to forward angles, i.e., $c(\pi - \theta)/c(\theta)$. The model fitting matches well with the experimental data above 1.4 a.u., as represented by the solid line in Fig. 7. A closer look at Fig. 7 shows that though the fitting matches well with the data, a periodic deviation is also observed. In order to study the deviations, we have divided the data points by the first-order fitting function (see the inset). The resulting data reveal an oscillatory structure which is further fitted by a model (solid line), similar to the Cohen-Fano-type formalism,

$$R_N = D + E \frac{\sin(nkd)}{nkd}, \quad (11)$$

where n is the frequency of oscillation, which is found to be 1.8, i.e., almost twice the frequency of the primary oscillation. This clearly indicates the presence of a higher-order contribution arising from a second-order scattering mechanism [24,25,41].

V. CONCLUSION

We have measured the absolute DDCS of the secondary electron emission in ionization of the N_2 molecule under the impact of fast electrons (7 keV) for emission angles between 15° and 145° . Experimental data have been compared with the theoretical calculations based on the B1 model, under the CNDO approximation with two different values of effective charges. The experimental-to-theoretical DDCS ratios (i.e., $N_2/2N$) were calculated using two different values of Z_T . The ratios show an oscillatory structure due to the Young-type interference, whose shape was found to be dependent on the choice of Z_T . Though in the case of $Z_T = 1$ the DDCS ratios revealed clear oscillations, for $Z_T = Z_{bk}$ the ratios had to be normalized by a linear function to deduce the oscillations clearly. The ratios have been fitted with the Cohen-Fano

model for either case. The derived values of the frequency parameter are seen to be constant for all forward angles and increase for backward angles. The forward-backward angular asymmetry displayed the oscillation very clearly and the fitting function based on the Cohen-Fano model matches well with the experimental ratio. However, periodic deviation from the first-order function indicates the presence of a second-order interference effect. It should be emphasized that since the asymmetry parameter is free from experimental normalization

procedure and does not require any theoretical atomic N cross section, it therefore provides a more convincing proof of the oscillation.

ACKNOWLEDGMENTS

The authors would like to thank D. Misra for the helpful discussions and also acknowledge the help of W. A. Fernandes and Nilesh Mhatre during the experiment.

-
- [1] C. B. Opal, W. K. Peterson, and E. C. Beaty, *J. Chem. Phys.* **55**, 4100 (1971).
- [2] T. D. Mark, *J. Chem. Phys.* **63**, 3731 (1975).
- [3] H. D. Cohen and U. Fano, *Phys. Rev.* **150**, 30 (1966).
- [4] N. Stolterfoht, B. Sulik, V. Hoffmann, B. Skogvall, J. Y. Chesnel, J. Rangama, F. Fremont, D. Hennecart, A. Cassimi, X. Husson, A. L. Landers, J. A. Tanis, M. E. Galassi, and R. D. Rivarola, *Phys. Rev. Lett.* **87**, 023201 (2001).
- [5] N. Stolterfoht, B. Sulik, L. Gulyás, B. Skogvall, J. Y. Chesnel, F. Frémont, D. Hennecart, A. Cassimi, L. Adoui, S. Hossain, and J. A. Tanis, *Phys. Rev. A* **67**, 030702(R) (2003).
- [6] D. Misra, U. Kadhane, Y. P. Singh, L. C. Tribedi, P. D. Fainstein, and P. Richard, *Phys. Rev. Lett.* **92**, 153201 (2004).
- [7] S. Chatterjee, D. Misra, A. H. Kelkar, Lokesh C. Tribedi, C. R. Stia, O. A. Fojón, and R. D. Rivarola, *J. Phys. B: At. Mol. Opt. Phys.* **42**, 065201 (2009).
- [8] S. Chatterjee, D. Misra, P. D. Fainstein, and L. C. Tribedi, *Phys. Scr.* **T144**, 014040 (2011).
- [9] D. Akoury, K. Kreidi, T. Jahnke, Th. Weber, A. Staudte, M. Schoffler, N. Neumann, J. Titze, L. Ph. H. Schmidt, A. Czasch, O. Jagutzki, R. A. Costa Fraga, R. E. Grisenti, R. Díez Muino, N. A. Cherepkov, S. K. Semenov, P. Ranitovic, C. L. Cocke, T. Osipov, H. Adaniya, J. C. Thompson, M. H. Prior, A. Belkacem, A. L. Landers, H. Schmidt-Bocking, and R. Dorner, *Science* **318**, 949 (2007).
- [10] D. S. Milne-Brownlie, M. Foster, Junfang Gao, B. Lohmann, and D. H. Madison, *Phys. Rev. Lett.* **96**, 233201 (2006).
- [11] S. E. Canton, E. Plésiat, J. D. Bozek, B. S. Rude, P. Decleva, and F. Martin, *Proc. Natl. Acad. Sci. USA* **108**, 7302 (2011).
- [12] J. L. Baran, S. Das, F. Járai-Szábo, K. Póra, L. Nagy, and J. A. Tanis, *Phys. Rev. A* **78**, 012710 (2008).
- [13] M. Winkworth, P. D. Fainstein, M. E. Galassi, J. L. Baran, B. S. Dassanayake, S. Das, A. Kayani, and J. A. Tanis, *Nucl. Instrum. Methods Phys. Res., Sect. B* **267**, 373 (2009).
- [14] H. Chaluvadi, N. O. Zehra, M. Dogan, C. Ning, J. Colgan, and D. Madison, *J. Phys. B* **48**, 155203 (2015).
- [15] L. R. Hargreaves, C. Colyer, M. A. Stevenson, B. Lohmann, O. Al-Hagan, D. H. Madison, and C. G. Ning, *Phys. Rev. A* **80**, 062704 (2009).
- [16] S. Nandi, S. Biswas, C. A. Tachino, R. D. Rivarola, and L. C. Tribedi, *Eur. Phys. J. D* **69**, 192 (2015).
- [17] S. Nandi, A. N. Agnihotri, S. Kasthurirangan, A. Kumar, C. A. Tachino, R. D. Rivarola, F. Martín, and L. C. Tribedi, *Phys. Rev. A* **85**, 062705 (2012).
- [18] M. Ilchen, L. Glaser, F. Scholz, P. Walter, S. Deinert, A. Rothkirch, J. Seltmann, J. Viehhaus, P. Decleva, B. Langer, A. Knie, A. Ehresmann, O. M. Al-Dossary, M. Braune, G. Hartmann, L. C. Tribedi, A. Meissner, M. AlKhalidi, and U. Becker, *Phys. Rev. Lett.* **112**, 023001 (2014).
- [19] D. Rolles *et al.*, *Nature (London)* **437**, 711 (2005).
- [20] B. Zimmermann *et al.*, *Nat. Phys.* **4**, 649 (2008).
- [21] S. K. Semenov *et al.*, *J. Phys. B: At. Mol. Opt. Phys.* **39**, L261 (2006).
- [22] X. J. Liu *et al.*, *J. Phys. B: At. Mol. Opt. Phys.* **39**, 4801 (2006).
- [23] K. Ueda *et al.*, *Chem. Phys.* **329**, 329 (2006).
- [24] N. Stolterfoht, B. Sulik, B. Skogvall, J. Y. Chesnel, F. Frémont, D. Hennecart, A. Cassimi, L. Adoui, S. Hossain, and J. A. Tanis, *Phys. Rev. A* **69**, 012701 (2004).
- [25] D. Misra, A. H. Kelkar, S. Chatterjee, and L. C. Tribedi, *Phys. Rev. A* **80**, 062701 (2009).
- [26] C. A. Tachino, F. Martin, and R. D. Rivarola, *J. Phys. B* **45**, 025201 (2012).
- [27] A. Kumar, D. Misra, K. V. Thulasiram, L. C. Tribedi, and A. K. Pradhan, *Nucl. Instrum. Methods B* **248**, 247 (2006).
- [28] Deepankar Misra, K. V. Thulasiram, W. Fernandes, Aditya H. Kelkar, U. Kadhane, Ajay Kumar, Yeshpal Singh, L. Gulyas, and Lokesh C. Tribedi, *Nucl. Instrum. Methods Phys. Res., Sect. B* **267**, 157 (2009).
- [29] B. Senger, E. Wittendorp-Rechenmann, and R. V. Rechenmann, *Nucl. Instrum. Methods Phys. Res.* **194**, 437 (1982).
- [30] J. A. Pople, D. P. Santry, and G. A. Segal, *J. Chem. Phys.* **43**, S129 (1965).
- [31] C. W. Scherr, *J. Chem. Phys.* **23**, 569 (1955).
- [32] K. Siegbahn, C. Nordling, G. Johansson, J. Hedman, P. F. Hedén, K. Hamrin, U. Gelius, T. Bergmark, L. O. Werme, R. Manne, and Y. Baer, *ESCA Applied to Free Molecules* (North Holland, Amsterdam, 1969).
- [33] P. D. Fainstein, V. H. Ponce, and R. D. Rivarola, *J. Phys. B: At. Mol. Opt. Phys.* **21**, 287 (1988).
- [34] E. Clementi and C. Roetti, *At. Data Nucl. Data Tables* **14**, 177 (1974).
- [35] D. Belkić, R. Gayet, and A. Salin, *Phys. Rep.* **56**, 279 (1979).
- [36] M. F. Ciappina, O. A. Fojon, and R. D. Rivarola, *J. Phys. B* **47**, 042001 (2014).
- [37] L. Nagy, L. Kocbach, K. Pora, and J. Hansen, *J. Phys. B* **35**, L453 (2002).

- [38] D. Misra, A. Kelkar, U. Kadhane, A. Kumar, L. C. Tribedi, and P. D. Fainstein, *Phys. Rev. A* **74**, 060701(R) (2006).
- [39] P. D. Fainstein, L. Gulyás, F. Martin, and A. Salin, *Phys. Rev. A* **53**, 3243 (1996).
- [40] D. Misra, A. Kelkar, U. Kadhane, A. Kumar, Y. P. Singh, L. C. Tribedi, and P. D. Fainstein, *Phys. Rev. A* **75**, 052712 (2007).
- [41] A. Messiah, *Quantum Mechanics* (North-Holland, Amsterdam, 1970), Vol. II, pp. 848–852.